



## Supporting Online Material for

### **Confined Crystallization of Polyethylene Oxide in Nanolayer Assemblies**

Haopeng Wang, Jong K. Keum, Anne Hiltner,\* Eric Baer,  
Benny Freeman, Artur Rozanski, Andrzej Galeski

\*To whom correspondence should be addressed. E-mail: ahiltner@case.edu

Published 6 February 2009, *Science* **323**, 757 (2009)

DOI: 10.1126/science.1164601

#### **This PDF file includes:**

Materials and Methods

SOM Text

Figs. S1 to S5

Tables S1 and S2

References

Supporting Online Material for  
Confined Crystallization of Polyethylene Oxide  
in Nanolayer Assemblies

*Haopeng Wang,<sup>1</sup> Jong K. Keum,<sup>1</sup> Anne Hiltner,<sup>1\*</sup> Eric Baer,<sup>1</sup> Benny Freeman,<sup>2</sup> Artur  
Rozanski,<sup>3</sup> Andrzej Galeski<sup>3</sup>*

<sup>1</sup>Department of Macromolecular Science and Engineering, Case Western Reserve  
University, Cleveland, OH 44106-7202

<sup>2</sup>Department of Chemical Engineering, University of Texas at Austin, Austin, TX 78758

<sup>3</sup>Centre of Molecular and Macromolecular Studies, Polish Academy of Sciences, 90-363  
Lodz, Poland

\*Corresponding author: Anne Hiltner (E-mail: [ahiltner@case.edu](mailto:ahiltner@case.edu))

Content of SOM  
Materials and methods  
SOM text  
Figure S1 to S5  
Table S1 to S2

## Materials

Poly(ethylene oxide) (PEO) with molecular weight of 200 kg/mol (PolyOx WSR N80) and ethylene acrylic acid copolymer (EAA) with 9.7 wt% acrylic acid (Primacor1410) were obtained from The Dow Chemical Company. Both EAA and PEO were dried under vacuum before processing.

## Methods

Films with alternating layers of PEO and EAA with EAA outer layers were fabricated using the layer multiplication process (S1, S2). The schematic drawing of layer-multiplying coextrusion in **Figure S1** shows how a series of  $n$  multiplying elements combines two dissimilar polymers as  $2^{(n+1)}+1$  alternating layers. The extruder, multipliers and die temperatures were set to 190 °C to ensure matching viscosities of the two polymer melts. Multilayered films with 33, 257 and 1025 alternating EAA and PEO layers were coextruded as films of various thicknesses and various composition ratios (vol/vol) including (EAA/PEO) 50/50, 70/30, 80/20 and 90/10. The nominal layer thickness was calculated from the number of layers, the composition ratio and the film thickness (**Table S1**). The films were stored at ambient temperature in desiccators to prevent moisture absorption.

Oxygen permeability at 23°C, 0% relative humidity and 1 atm pressure was measured with a MOCON OX-TRAN 2/20. The instrument was calibrated with National Institute of Standards and Technology certified Mylar film of known O<sub>2</sub> transport characteristics. The specimens were carefully conditioned in the instrument, as described previously (S3). The O<sub>2</sub> permeability  $P$  was calculated from the steady state flux  $J$  as

$$P = J \frac{l}{\Delta p} \quad (\text{S1})$$

where  $l$  is the film thickness and  $\Delta p$  is the difference of the oxygen partial pressure across the film. For each film, the average  $P$  from two specimens is reported.

Differential scanning calorimetry (DSC) was conducted with a Perkin-Elmer DSC-7 at a heating rate  $10\text{ }^{\circ}\text{C min}^{-1}$ . The film density was determined by hydrostatic weighing using a balance and a density determination kit (Mettler Toledo Model XS205). Iso-octane (99.8 % pure, Sigma Aldrich) with density of  $0.692\text{ g cm}^{-3}$  was used as the auxiliary liquid (S4). The density of the EAA film was  $0.936\text{ g cm}^{-3}$  and that of the PEO film was  $1.217\text{ g cm}^{-3}$ .

Embedded films were microtomed through the thickness at  $-75\text{ }^{\circ}\text{C}$  with a cryo-ultramicrotome (MT6000-XL from RMC) and cross-sections were examined with an atomic force microscope (AFM) in order to visualize the layers and the layer morphology. Phase and height images of the cross-section were recorded simultaneously at ambient temperature in air using the tapping mode of the Nanoscope IIIa MultiMode scanning probe (Digital Instruments).

Small-angle X-ray scattering (SAXS) and wide-angle X-ray scattering (WAXS) patterns were obtained by aligning the incident X-ray beam parallel to the normal direction (ND), the extrusion direction (ED) and the transverse direction (TD) of the film. SAXS measurements were carried out using a rotating anode X-ray generator (Rigaku RU 300, 12 kW) equipped with two laterally graded multilayer optics in a side-by-side arrangement, giving a highly focused parallel beam of monochromatic Cu  $K\alpha$  radiation ( $\lambda = 0.154\text{ nm}$ ). The monochromatic X-ray beam operated at 50 kV and 100 mA was

collimated using three pinholes and the diameter of X-ray beam at sample position was approximately 700  $\mu\text{m}$ . For the collection of ED and TD SAXS patterns, since the dimensions of the films (42~282  $\mu\text{m}$  thick and 2 mm wide) were smaller than the collimated X-ray beam, the X-ray beam was aligned at an angle of  $\sim 3^\circ$  relative to ED and TD to avoid total reflection. The critical angle for the total reflection is usually on the order of a few tenths of a degree. On the other hand, in order to collect ND SAXS patterns, the X-ray beam was aligned along the direction parallel to the ND. Two dimensional (2D) SAXS patterns were collected by using a 2D gas filled multiwire detector (Rigaku) with a spatial resolution of  $1024 \times 1024$  pixels. The X-ray exposure times for ED, TD and ND SAXS patterns were 9 hours. The sample-to-detector distance was 1.5 m and the scattering vector  $q$  was calibrated using a silver behenate (AgBe) standard, which had (001) peak position at  $q=1.076 \text{ nm}^{-1}$ . A beam stop placed in front of the area detector allowed monitoring of the intensity of the direct beam. Based on the intensity of the direct beam, all SAXS images were corrected for background scattering, dark current and sample absorption.

WAXS measurements were performed using a Statton camera coupled to a Philips PW 1830 X-ray generator (Cu  $K\alpha$  radiation,  $\lambda=0.154 \text{ nm}$ ) operated at 30 kV and 35 mA. The collimated beam diameter was 250  $\mu\text{m}$ . 2D WAXS images were collected using imaging plate and exposed imaging plates were read with a Fujifilm FDL5000 image plate reader. The sample-to-detector distance was 60 mm and the diffraction angle was calibrated using a  $\text{CaF}_2$  standard. Several film pieces were stacked and glued with isocyanate 10s glue. The thickness of the stack was approximately 0.5 mm. The stacks were exposed in the three orthogonal directions. For the ED and TD directions, the film

stack was sectioned perpendicular to the plane of the film to obtain a dimension of 1 mm in the X-ray beam direction.

The orientation of the crystalline phase of PEO was also studied by means of X-ray scattering with pole figures. For an overview of this technique see Ref.(S5) A WAXS system consisting of a computer-controlled pole figure device associated with a wide-angle goniometer coupled to a sealed tube X-ray generator operating at 50 kV and 30mA (Philips) was used in this study. The X-ray beam consisted of Cu K $\alpha$  radiation filtered electronically and by Ni filter. The specimens in the form of sandwiched films approx. 0.5 mm thick were assembled with extrusion direction vertical. The (120) and (032) crystal planes of commonly found monoclinic form of PEO were analyzed (diffraction maxima centered around  $2\theta = 19.2^\circ$  and  $23.3^\circ$ , respectively) and the respective pole figures were constructed. Experimental diffraction data were corrected for background scattering, sample absorption and defocusing of the beam. All pole figures were plotted with the POD program (Los Alamos National Lab, NM). Other details of the experimental procedure were described elsewhere (S6).

## Results and Discussion

**DSC analysis.** **Figure S2** shows the first melting thermograms of layered EAA/PEO films with total thickness of about 120  $\mu\text{m}$  and 1025 alternating layers, together with EAA and PEO control films. The PEO control film exhibited a sharp melting endotherm with peak melting temperature  $T_m$  at 65  $^\circ\text{C}$ . The EAA control film exhibited a broad melting endotherm with the melting peak at 97  $^\circ\text{C}$ . The crystallinity calculated from  $\Delta H_m$  was 78 wt% for PEO and 34 wt% for EAA using the heat of fusion

( $\Delta H^\circ$ ) values of 197 J g<sup>-1</sup> for PEO crystals (S7) and 290 J g<sup>-1</sup> for polyethylene crystals (S8). All the layered films exhibited a melting peak for the EAA constituent at 97 °C in the heating thermograms, corresponding to the melting temperature that of the EAA control films. The peak melting temperature for the PEO constituent in the layered films was about 2~3°C lower than that of the PEO control film. The measured values of  $\Delta H_{m,total}$  of the layered films were close to the calculated additive value from film composition. Separation of the enthalpy contribution of the PEO layers ( $\Delta H_{m,PEO}$ ) from the total melting enthalpy ( $\Delta H_{m,total}$ ) was performed and the crystallinity of the PEO layers was calculated based on  $\Delta H_{m,PEO}$  and the PEO content in the films (**Table S2**). The crystallinity of PEO in the layers was close to that of the PEO control film.

**SAXS analysis.** **Figure S3** shows the 2-dimensional SAXS patterns of EAA/PEO films with 3.6  $\mu$ m, 110 nm and 20 nm PEO layers where the incident X-ray beam was parallel to the normal direction (ND) and to the extrusion direction (ED). Because the SAXS patterns measured in the transverse direction (TD) were indistinguishable from those in the ED, only ED and ND patterns are presented in the following discussion. The intense meridional streak in the ED patterns was mainly associated with grazing incidence scattering. This scattering was found to veil weak scattering from the lamellae. For clarification, the equatorial and meridional scattering profiles were extracted from the 2D patterns and are depicted in **Figure S4**. The peak assignments were based on the peak positions of the PEO and EAA control films in **Figure S4A**. Comparison of the various scattering profiles indicated that the first-order peak positions of the PEO and EAA lamellae in coextruded EAA/PEO films remained nearly the same as in the control films. The long periods,  $L_p=2\pi/q$ , for PEO and EAA

lamellae obtained from the SAXS measurements were  $22.0 \pm 0.6$  nm and  $10.8 \pm 0.5$  nm, respectively. The long period of PEO was consistent with literature reports for this molecular weight (S9).

The ND and ED profiles from 3.6  $\mu\text{m}$  PEO layers (**Figure S4B**) showed almost the same peak sharpness and height as the PEO control films implying that the PEO layers were too thick for PEO lamellae to feel any significant confinement effect. The slight increase in the meridional intensity over the equatorial intensity in the ND patterns was attributed to the melt flow during coextrusion.

As the PEO layer thickness decreased to 110 nm and 20 nm (**Figure S4C and D**, respectively), highly oriented scattering features of the PEO lamellae appeared. These were due to the spatial confinement, not to a mechanical flow effect. The scattering peak of PEO lamellae in the ED meridional pattern was much stronger and sharper than in the ED equatorial pattern, where it was barely discernable. Also, no first-order peak maximum for the PEO lamellae was discerned in the ND patterns. These scattering features implied that large-scale, oriented structures with the main scattering vector normal to the layer formed in the PEO layers. This was evidence that PEO lamellae were oriented primarily parallel to the layer surface. Crystallization as in-plane lamellae was due to the narrow confinement in the EAA layer interstices. The well-oriented, in-plane lamellae were not detected when the X-ray beam was parallel to the ND since this direction was along the projection direction of the lamellar stacks. The in-plane lamellae were totally different from the individual lamellae of a shish-kebab or a spherulite, which have only one growth face. Rather, they were more like single crystals.

Scattering from the 20 nm PEO layers was only detected on the meridian with the X-ray beam parallel to the ED. This implied a single population of in-plane lamellae that had grown in the direction parallel to the PEO layers. It was also noted that the first order peak maxima in the SAXS pattern from 20 nm layers was much weaker than that from 110 nm layers. If the lamellae were uncorrelated within the PEO layers, they should not show a first-order peak maximum in the SAXS pattern, and rather, should exhibit only single lamellar scattering features. Thus, it was thought that the observed weak lamellar correlation peak from 20 nm PEO layers was associated with the thickness distribution of the layers which occasionally enabled formation of two single crystals in a single PEO layer.

In contrast to the high degree of lamellar orientation in the PEO layers, the broad EAA first order SAXS reflection appeared in the ED and TD patterns with only a slight meridional concentration, which was especially evident in the ND profiles. The slight residual orientation of the EAA lamellae was attributed to the melt flow during coextrusion.

**WAXS Analysis.** The 2-dimensional transmission WAXS patterns from EAA and PEO films confirmed that EAA had the orthorhombic crystal form of polyethylene, and PEO took the usual monoclinic crystal form. The WAXS patterns of EAA/PEO layered films are shown in **Figure S5**. Because the WAXS patterns measured in the TD were indistinguishable from those in the ED, only ED and ND patterns are presented here. The EAA (110) reflection (scattering angle  $2\theta = 21.5^\circ$ ), and the PEO (120) reflection ( $2\theta = 19.2^\circ$ ) and (032) reflection ( $2\theta = 23.3^\circ$ ) appear in the WAXS patterns (*S10*). The EAA (200) reflection ( $2\theta = 23.6^\circ$ ), which was seen in the EAA pattern, was

superimposed on the stronger PEO (032) reflection. The ND and ED patterns from the coextruded films with 3.6  $\mu\text{m}$ -thick PEO layers exhibited almost isotropic rings for reflections from both the PEO and the EAA layers, **Figure S5A**.

The ED pattern from the film with 110 nm PEO layers (**Figure S5B**) revealed considerable orientation of the PEO. The PEO (120) reflections appeared as equatorial arcs and the PEO (032) reflections as arcs at approximately  $+65^\circ$  and  $-65^\circ$  with respect to the vertical direction. In addition, the  $(\bar{2}24)$  and (024) reflections appeared at  $+45^\circ$  and  $-45^\circ$  with respect to the vertical direction. Decreasing the PEO layer thickness to 20 nm sharpened the arcs in the ED pattern to spots, **Figure S5C**. The ED pattern resembled the PEO fiber pattern (S11) and indicated that the  $c$ -axis of the PEO crystals was oriented along the ND, i.e. vertical to the layer plane.

The ND patterns from the 110 nm and 20 nm PEO layers showed strong scattering at all angles, suggesting that the lamellae were essentially randomly oriented in the layer plane. In contrast to the high degree of orientation in the PEO layers, the EAA (110) reflection appeared as an almost isotropic ring in the ED patterns with only a slight equatorial concentration in the ND pattern due to slight orientation of the EAA chains in the extrusion direction. No other specific orientation of the EAA crystallographic planes was observed, although the EAA layers in these two samples were less than 400 nm thick. It was highly unlikely that the slight residual orientation of EAA from the extrusion process affected the oxygen permeability.

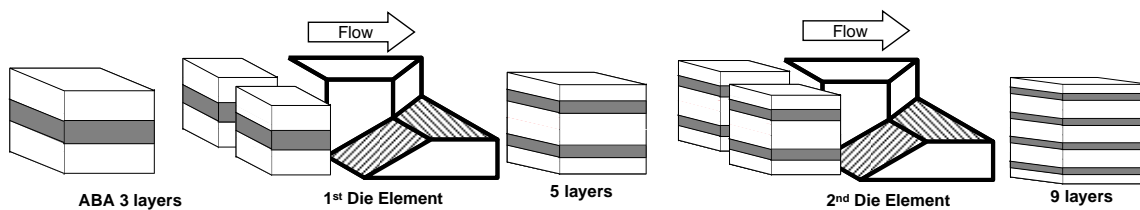


**Figure S1.** Layer-multiplying coextrusion for forced-assembly of polymer nanolayers. After the polymer melts are combined in the ABA feedblock, the melt stream flows through a series of layer-multiplying die elements; each element splits the melt vertically, spreads it horizontally, and finally recombines it with twice the number of layers. The figure illustrates how two elements multiply the number of layers from 3 to 9. An assembly of  $n$  die elements produces  $2^{(n+1)}+1$  layers with polymer A layers on both sides of the film. Finally, the melt is spread in a film die to further reduce the layer thickness.

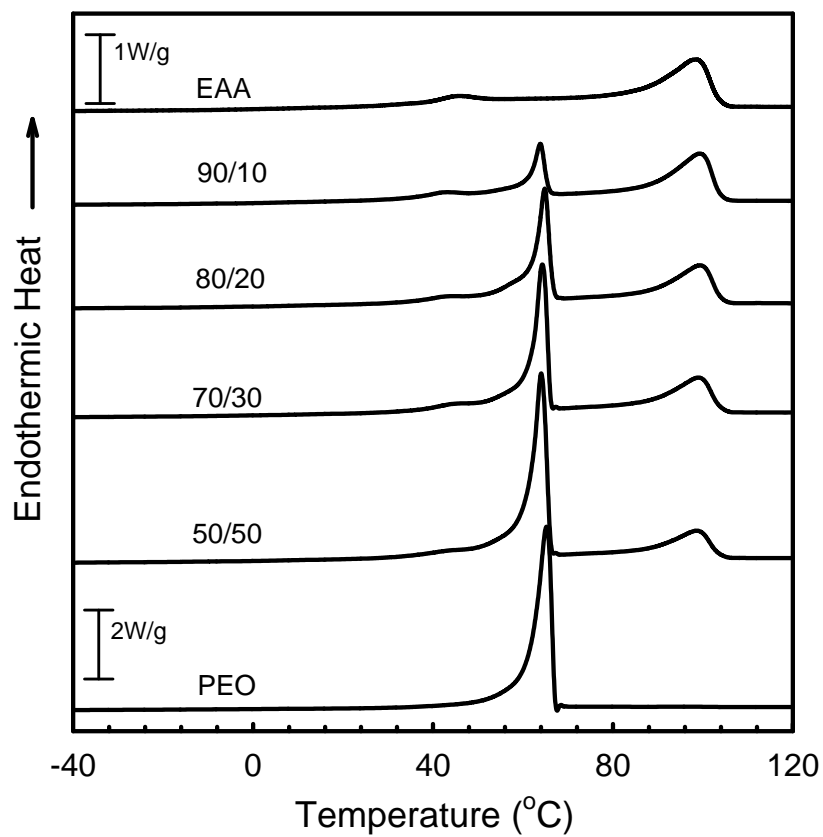


**Figure S2** The first heating thermograms of EAA/PEO films with 1025 alternating layers and total thickness about 120 $\mu$ m. The EAA/PEO compositions (v/v) are as labeled. The heating rate was 10°C/min.

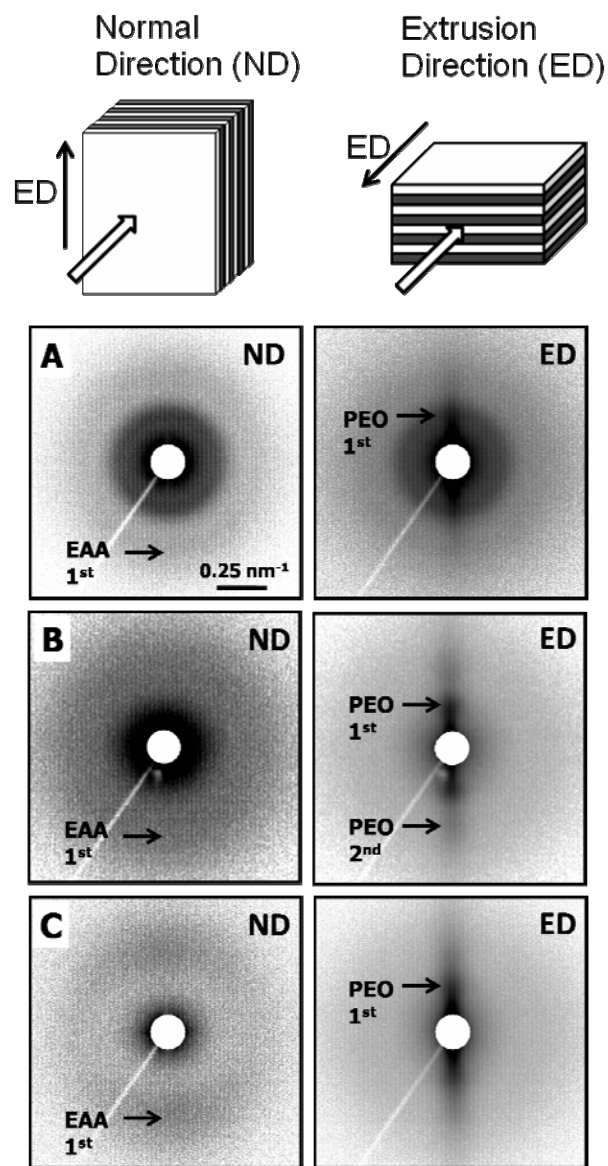


**Figure S3** The 2D SAXS patterns of EAA/PEO films with different PEO layer thicknesses. The patterns were measured along the normal direction (ND) and the extrusion direction (ED): (A) 3.6  $\mu\text{m}$  PEO layers; (B) 110 nm PEO layers; and (C) 20 nm PEO layers. The PEO first-order, PEO second-order and EAA first-order peaks are marked with arrows. The scale bar in (A) defines the scattering vector  $q$  scale. The intense meridional streak in the ED patterns is due to grazing incidence scattering.

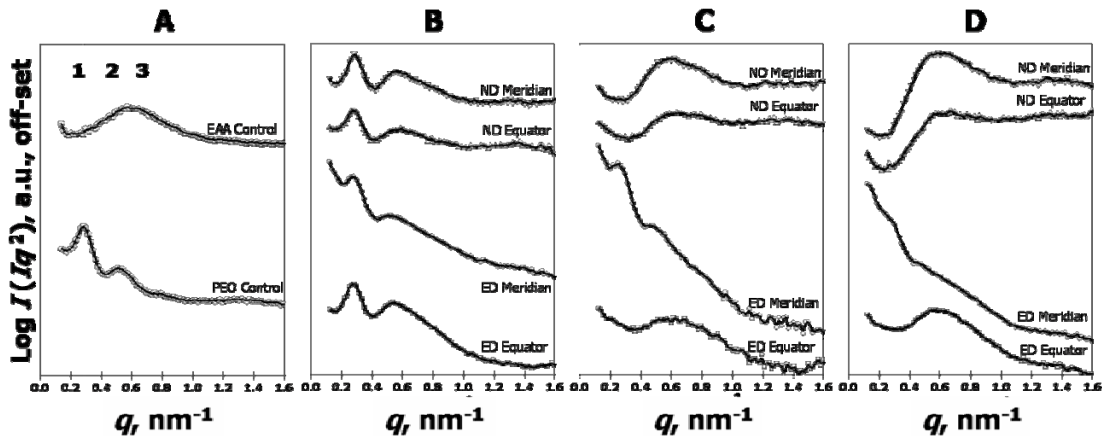


**Figure S4** The 1D equatorial and meridional SAXS slices were extracted from the 2D images. (A) The control films showed the first and second order PEO small-angle reflections and the first order EAA reflection, which are indicated by the vertical lines. (B) The ND and ED profiles from the 3.6  $\mu\text{m}$  PEO layers show almost the same peak sharpness and height as the PEO control indicating that the PEO layers are essentially isotropic and too thick for the lamellae to feel any significant confinement effect. (C) Strong small-angle scattering from 110nm PEO layers only in the ED meridional slice shows that the PEO lamellae are oriented primarily in the plane of the layer. (D) Weak small-angle PEO scattering from 20 nm layers in the ED meridional slice suggests primarily single, isolated lamellae.

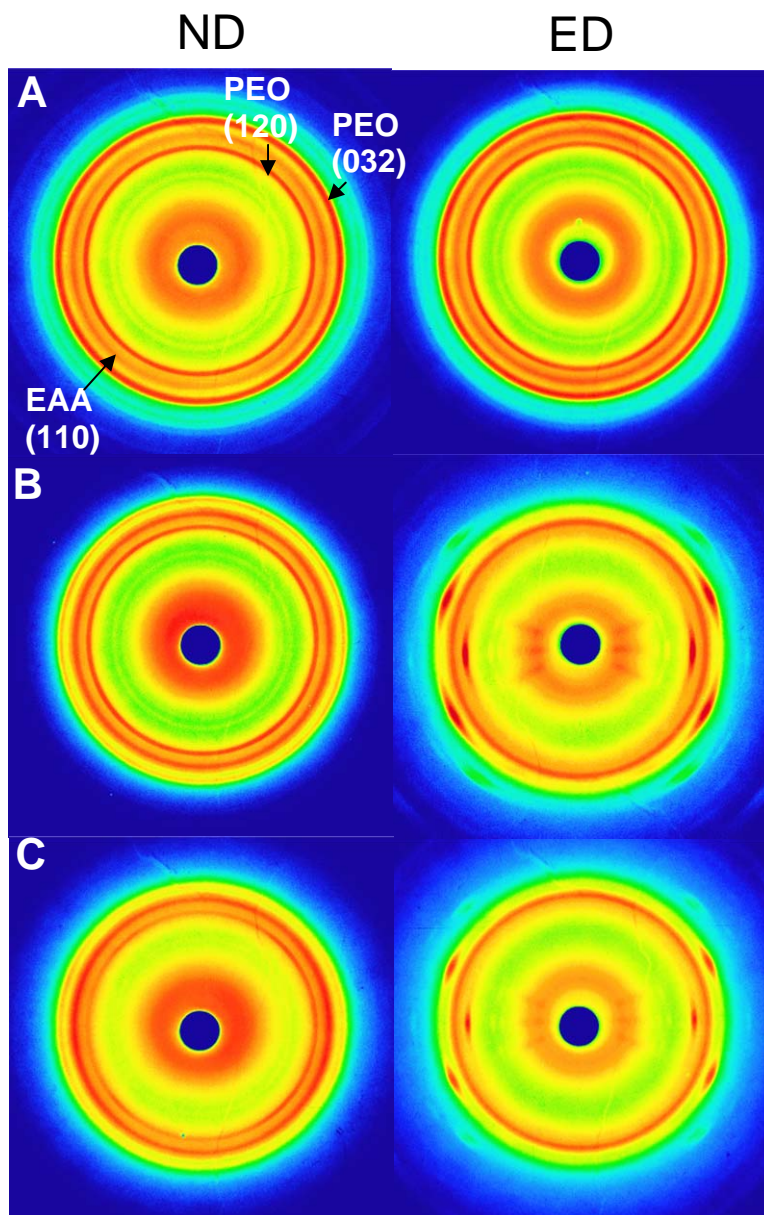


**Figure S5** The 2D WAXS patterns of EAA/PEO films with different PEO layer thicknesses. (A) The ND and ED patterns from the 3.6  $\mu\text{m}$  PEO layers confirm the usual monoclinic crystal form of PEO and show the isotropic orientation of the unit cell. (B) The ND and ED patterns from the 110 nm PEO layers show a high degree of orientation with the  $c$ -axis vertical to the layer plane. (C) Arcs in the WAXS ED pattern of 110 nm PEO layers are sharpened to spots in the WAXS ED pattern of 20 nm PEO layers.

**Table S1 Film composition, number of layers, film thickness and nominal PEO layer thickness of EAA/PEO films**

<b>EAA/PEO</b> <b>(v/v)</b>	<b>Number</b> <b>of layers</b>	<b>Film</b> <b>Thickness</b> <b>(<math>\mu\text{m}</math>)</b>	<b>Nominal PEO</b> <b>layer Thickness</b> <b>(nm)</b>
0/100	1025	110	--
50/50	33	115	3600
70/30	33	110	2060
50/50	257	282	1100
50/50	257	130	510
70/30	257	120	280
50/50	257	46	180
50/50	1025	127	125
70/30	1025	190	110
70/30	257	38	90
70/30	1025	119	70
80/20	1025	133	50
50/50	1025	47	45
70/30	1025	51	30
80/20	1025	61	25
90/10	1025	107	20
90/10	1025	42	8
100/0	1025	121	--

**Table S2 Melting enthalpies of EAA/PEO films with 1025 alternating layers**

<b>EAA/PEO</b>		<b>Film</b>	<b>Nominal</b>	$\Delta H_{m, EAA}^a$	$X_{c, EAA}^b$	$\Delta H_{m, PEO}^c$	$X_{c, PEO}^d$
<b>(v/v)</b>	<b>(wt/wt)</b>	<b>Thickness</b>	<b>PEO Layer Thickness</b>				
		<b>(<math>\mu\text{m}</math>)</b>	<b>(nm)</b>	<b>(J/g)</b>	<b>(wt%)</b>	<b>(J/g)</b>	<b>(wt%)</b>
100/0	100/0	121	--	98	34	--	--
90/10	87/13	107	20	98	34	138	70
80/20	75/25	133	50	96	33	156	79
70/30	64/36	119	70	102	35	150	76
50/50	43/57	127	125	102	35	144	73
0/100	0/100	110	--	--	--	153	78

<sup>a</sup> heat of melting normalized to the weight fraction of the EAA layers

<sup>b</sup> calculated crystallinity of the EAA layers

<sup>c</sup> heat of melting normalized to the weight fraction of the PEO layers

<sup>d</sup> calculated crystallinity of PEO the layers

## References

- S1 C. D. Mueller, S. Nazarenko, T. Ebeling, T. L. Schuman, A. Hiltner, E. Baer, *Polym. Eng. Sci.* **37**, 355-362 (1997).
- S2 T. E. Bernal-Lara, A. Ranade, A. Hiltner, E. Baer, in *Mechanical Properties of Polymers Based on Nanostructure*, 1st edition, G. H. Micheler, F. Balta-Callaja, Eds. (CRC press, Boca Raton, Florida 2005), pp. 629-682.
- S3 D. J. Sekelik, E. V. Stepanov, S. Nazarenko, D. Schiraldi, A. Hiltner, E. Baer, *J. Polym. Sci. Pt. B-Polym. Phys.* **37**, 847-857 (1999).
- S4 H. Lin, B. D. Freeman, *J. Membrane Sci.* **239**, 105 (2004).
- S5 L. E. Alexander, *X-Ray Diffraction Methods in Polymer Science* (Wiley: New York, 1969).
- S6 M. Pluta, Z. Bartczak, A. Galeski, *Polymer* **41**, 2271-2288 (2000)
- S7 C. Campbell, K. Viras, M. J. Richardson, A. J. Masters, C. Booth, *Makromol. Chem.* 1993, 194, 799.
- S8 Wunderlich, B. *Macromolecular Physics*, Vol. 3; Academic Press: New York, 1980, 42.
- S9 L. Zhao, W. Kai, Y. He, B. Zhu, Y. Inoue *J. Polym. Sci. Part B: Polym. Phys.* **43**, 2665-2676 (2005)
- S10 The PEO reflection labeled (032) actually contains overlapped reflections from (032), ( $\bar{1}32$ ), (112), ( $\bar{2}12$ ), ( $\bar{1}24$ ), ( $\bar{2}04$ ) and (004) which have similar  $d$ -spacing of  $\sim 0.39\text{nm}$  with that from (032) being the strongest. They cannot be easily separated in (032) pole figure. Details can be found in L. Zhu et al, *J. Am. Chem. Soc.* **122**, 5957-5967 (2000).
- S11 Y. Takahashi, H. Tadokoro, *Macromolecules* **6**, 672-675 (1973).